Asoke K. Nandi
N. Sujatha · R. Menaka
John Sahaya Rani Alex *Editors*

Computational Signal Processing and Analysis

Select Proceedings of ICNETS2, Volume I

Springer

Lecture Notes in Electrical Engineering

Volume 490

Lecture Notes in Electrical Engineering (LNEE) is a book series which reports the latest research and developments in Electrical Engineering, namely:

- Communication, Networks, and Information Theory
- Computer Engineering
- Signal, Image, Speech and Information Processing
- Circuits and Systems
- Bioengineering
- Engineering

The audience for the books in LNEE consists of advanced level students, researchers, and industry professionals working at the forefront of their fields. Much like Springer's other Lecture Notes series, LNEE will be distributed through Springer's print and electronic publishing channels.

For general information about this series, comments or suggestions, please use the contact address under "service for this series".

To submit a proposal or request further information, please contact the appropriate Springer Publishing Editors:

Asia:

China, *Jessie Guo, Assistant Editor* (jessie.guo@springer.com) (Engineering)

India, *Swati Meherishi, Senior Editor* (swati.meherishi@springer.com) (Engineering)

Japan, *Takeyuki Yonezawa, Editorial Director* (takeyuki.yonezawa@springer.com) (Physical Sciences & Engineering)

South Korea, *Smith (Ahram) Chae, Associate Editor* (smith.chae@springer.com) (Physical Sciences & Engineering)

Southeast Asia, *Ramesh Premnath, Editor* (ramesh.premnath@springer.com) (Electrical Engineering)

South Asia, *Aninda Bose, Editor* (aninda.bose@springer.com) (Electrical Engineering)

Europe:

Leontina Di Cecco, Editor (Leontina.dicecco@springer.com) (Applied Sciences and Engineering; Bio-Inspired Robotics, Medical Robotics, Bioengineering; Computational Methods & Models in Science, Medicine and Technology; Soft Computing; Philosophy of Modern Science and Technologies; Mechanical Engineering; Ocean and Naval Engineering; Water Management & Technology)

(christoph.baumann@springer.com) (Heat and Mass Transfer, Signal Processing and Telecommunications, and Solid and Fluid Mechanics, and Engineering Materials)

North America:

Michael Luby, Editor (michael.luby@springer.com) (Mechanics; Materials)

More information about this series at http://www.springer.com/series/7818

Asoke K. Nandi · N. Sujatha
R. Menaka · John Sahaya Rani Alex
Editors

Computational Signal Processing and Analysis

Select Proceedings of ICNETS2, Volume I

Springer

Editors
Asoke K. Nandi
Department of Electronic and Computer
    Engineering
Brunel University London
Uxbridge
UK

N. Sujatha
Department of Applied Mechanics
Indian Institute of Technology Madras
Chennai, Tamil Nadu
India

R. Menaka
School of Electronics Engineering
VIT University
Chennai, Tamil Nadu
India

John Sahaya Rani Alex
School of Electronics Engineering
VIT University
Chennai, Tamil Nadu
India

Preface

This LNEE volume consists of papers presented at the Symposium-A entitled "Computational Signal Processing and Analysis" in the International Conference on "NextGen Electronic Technologies–Silicon to Software"—ICNETS[2]-2017, which was held in VIT Chennai, India, during 23–25 March 2017.

The focus of this symposium was to bring together researchers and technologists working in different aspects of signal processing such as biomedical signal processing, image processing and video processing. One of the major objectives of this symposium is to highlight the current research developments in the areas of signal, image and video processing.

This symposium received over 64 paper submissions from various countries across the globe. After a rigorous peer review process, 37 full-length papers were accepted for presentation at the conference. This was intended to maintain the high standards of the conference proceedings. The presented papers were oriented towards addressing challenges involved in different application areas of signal processing. In addition to the contributed papers, renowned domain experts across the globe were invited to deliver keynote speeches at ICNETS[2]-2017.

The session chairs of different sessions played key roles in conducting the proceedings of each session in a well-organized manner.

We would like to recognize Springer LNEE for publishing the proceedings of Symposium-A as one volume. We would also like to thank the ICNETS^2-2017 Secretariat for dexterity. We would like to place on record the tireless work contributed by Symposium-A manager Dr. Jagannath. We acknowledge our publication committee Dr. Mohanaprasad, Dr. Annis Fathima and Dr. Velmathi for their efforts. Finally, we would like to show appreciation to our signal processing research group faculty members for their several months of hard work in making this symposium a prolific one.

Uxbridge, UK   Asoke K. Nandi
Chennai, India   N. Sujatha
Chennai, India   R. Menaka
Chennai, India   John Sahaya Rani Alex

Contents

About the Editors

Prof. Asoke K. Nandi received his Ph.D. degree from the University of Cambridge (Trinity College). He has held positions at the University of Oxford, Imperial College London, the University of Strathclyde and the University of Liverpool. In 2013, he moved to Brunel University London as the Head of Electronic and Computer Engineering. In 1983, his co-discovery of the three particles (W+, W− and Z0) was recognized by the Nobel Committee for Physics in 1984. He has made numerous fundamental contributions to signal processing and machine learning and has authored over 550 technical publications, with an h-index of 67. He is a fellow of the Royal Academy of Engineering, UK, and of seven other institutions including IEEE. Among the many awards he has received are the IEEE Heinrich Hertz Award (2012), the Glory of Bengal Award for his outstanding achievements in scientific research (2010), the Institution of Mechanical Engineers Water Arbitration Prize (1999) and the Mountbatten Premium from the Institution of Electrical Engineers (1998).

Dr. N. Sujatha graduated in Biomedical Optics from Nanyang Technological University (NTU), Singapore, and is an Associate Professor at the Department of Applied Mechanics, IIT Madras, India. She has also served as a Visiting Associate Professor at NTU, Singapore, in 2014–2015. Her major research interests are laser-based diagnostic imaging and diagnostic optical spectroscopy. She has co-authored a chapter and published over 50 international journal/conference papers, several of which have won best paper awards. She is a member of International Society for Optical Engineering, Optical Society of America, and is a fellow of the Optical Society of India.

Dr. R. Menaka received her doctoral degree in Medical Image Processing from Anna University, Chennai, and is currently an Associate Professor at the School of Electronics Engineering, VIT University, Chennai. She has served in both industry and academia for more than 25 years and has published over 35 research papers in various national and international journals and conferences. Her areas of interest include signal and image processing, neural networks and fuzzy logic.

John Sahaya Rani Alex is an Associate Professor at the School of Electronics Engineering, VIT Chennai. She has worked in the embedded systems and software engineering fields for 12 years, which includes 7 years' experience in the USA. Her research interests include spoken utterance detection and implementations of digital signal processing (DSP) algorithms in an embedded system. She is a member of IEEE and the IEEE Signal Processing Society.

Detecting Happiness in Human Face Using Minimal Feature Vectors

Manoj Prabhakaran Kumar and Manoj Kumar Rajagopal

Abstract Human emotions estimated from face become more effective compared to various modes of extracting emotion owing to its robustness, high accuracy and better efficiency. This paper proposes detecting happiness of human face using minimal facial features from geometric deformable model and supervised classifier. First, the face detection and tracking is observed by constrained local model (CLM). Using CLM grid node, the entire and minimal feature vectors displacement is obtained by facial feature extraction. Compared to entire features, minimal feature vectors is considered for detecting happiness to improve accuracy. Facial animation parameters (FAPs) helps in identifying the facial feature movements to forms the feature vectors displacement. The feature vectors displacement is computed in supervised bilinear support vector machines (SVMs) classifier to detect the happiness in human frontal face image sequences. This paper focuses on minimal feature vectors of happiness (frontal face) in both training and testing phases. MMI facial expression database is used in training, and real-time data are used for testing phases. As a result, the overall accuracy of happiness is achieved 91.66% using minimal feature vectors.

M. P. Kumar (✉) · M. K. Rajagopal
School of Electronics Engineering, Vellore Institute of Technology,
Chennai, Tamil Nadu, India
e-mail: manoj.prabhakaran2013@vit.ac.in

M. K. Rajagopal
e-mail: manojkumar.r@vit.ac.in

1 Introduction

Since 1990s, several researches are carried out on human emotion recognition for human–computer interaction (HCI), affective computing, etc. Emotion recognition in human has been established by the various modes of extraction [1]: physiological signal and non-physiological signal. From [1], the facial expression recognition is best out of the various modes of extracting emotion methods. From 1990 to till now, researchers are mostly concentrating on the robust automatic facial expression from image sequence compared to other modes of extracting emotions. In [2] has given the study of automatic facial expression system, through the photographic stimuli. In [3, 4] has established the automatic facial expression system from facial image sequence, which analyze the facial emotion through feature detection and tracking points.

From the literature survey [5–10], it is observed that the facial emotions are defined by the maximum number of facial feature points with action units (AUs) [11]. Therefore, usage of more feature points for facial emotion attains the complex data computation with less accuracy. To overcome this problem, the minimal feature points are selected for human facial expression. Facial action coding system (FACS) defines the combination of action units for facial emotion, using the entire feature points. Facial animation parameters (FAPs) [12] define facial emotion of action units within 10 groups, which use the entire feature points. Therefore, FAPs are considered for emotions' extraction using minimal feature vectors, which result in less data computational with high accuracy.

From [13] explain the importance of face modeling: the state of art with respect to different face models of face detection, tracking of automatic facial expression recognition.

In this paper, the detecting happiness is based on constrained local model (CLM) and bilinear support vector machines (SVMs). CLM [14] is developed for the face detection, tracking, and extracting the feature points. The extracted feature points form the minimal feature vectors displacements. The bilinear SVMs [15, 16] are formulated for classification of detecting happiness with help of FAPs [12]. The rest of the paper is as follows: The descriptions of detecting happiness are shown in Sect. 2. Section 3 describes the experimental results and discussion of proposed system. Section 4 summarizes the future work and conclusion.

2 System Description

The system description of detecting happiness is followed in three steps: face detection, tracking and feature extraction. From the facial feature vectors displacement, facial expressions are classified. Face detection and tracking, are carried out using deformable geometric grid node (CLM) [14]. Then feature vectors displacement is composed in supervised classifier (SVMs) [15] for defining the
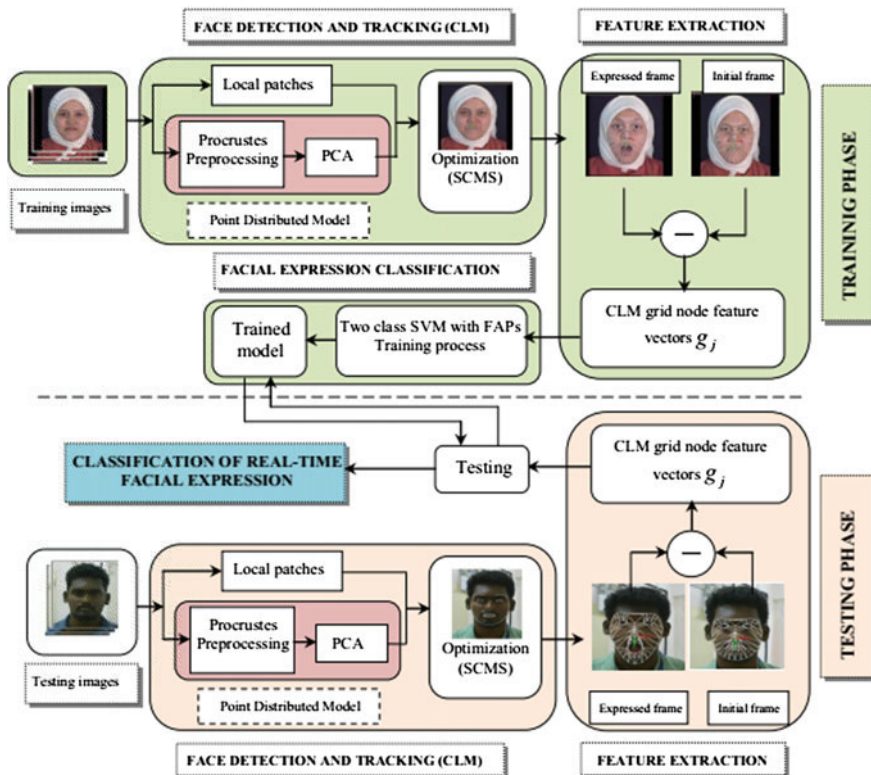
Fig. 1 Architecture of detecting happiness

happiness in human face. The proposed system architecture of detecting happiness is shown in Fig. 1.

2.1 Facial Detection and Tracking

In the proposed system, the face detection and tracking is carried out by constrained local model (CLM) (deformable geometric model fitting) [14], which represented two processes such as CLM model building and CLM search. The conceptual diagram of CLM model and search is as shown in Fig. 1.

2.1.1 Building a CLM Model

In CLM model building, there are two processes: shape model and patch model. In the shape model, first mark manually the landmark of feature points of face using

point distribution model (PDM) [17]. PDM employed the non-rigid face shape of 2D+3D vector mesh. In PDM (Eq. (1)), building with principal component analysis (PCA) and Procrustes preprocessing. Principal component analysis (PCA) is applied for alignment of shape from the large database to get the mean value and eigen vectors shape of face. Before PCA, applying the Procrustes analysis for removing the scale, rotation, translations and gives the result of aligned shape. Similarly, the patch model applying logistic regression gives the result of mean value and eigen vectors of patch model.

$$x_i = sR(\tilde{x}_i) + T_{t_x,t_y} \Leftarrow T_{s,R,t_x,t_y}(\tilde{x}_i) \tag{1}$$

where x_i mentioned as ith landmark of 2D+3D PDM's location, $\vec{x}_i$ identify as mean shape of 2D+3D PDM and pose parameters of PDM represent as $p = (s, R, t, q)$. s, R, t are denoted as shape, rotation, and translation.

2.2 Searching with CLM

In searching face with CLM, applying the linear logistic regressor algorithm for extracting the feature points of each face feature variation gives the response maps of ith image frames in Eq. (2).

$$p(l_i = \textbf{aligned}|I, \mathbf{x}) = \frac{1}{1 + \exp\{\alpha\, C_i(I; \mathbf{x}) + \beta\}} \tag{2}$$

From the each feature point, crop a patch image of individual part (i.e., nose, left eye, right eye) and apply the linear logistic regressor [14], which is trained model to finding the local region of image and gives the result of response image. The quadratic function is fit on the response image of feature point position by optimization function is subspace constrained mean shift (SCMA) [14]. The mean shift algorithm [18] is applied for landmark location with aligned shape and patches in Eq. (3).

$$x_i^{(\tau+1)} \leftarrow \sum_{\mu_i \in \psi_{x_i^c}} \frac{\alpha_{\mu_i}^i\, N\left(x_i^{(\tau)}; \mu_i, \sigma^2 I\right)}{\sum\limits_{y \in \psi_{x_i^c}} \alpha_y^i\, N\left(x_i^{(\tau)}; y, \sigma^2 I\right)} \mu_i \tag{3}$$

Finally, combining a shape constraint model and local region of optimization function obtains the feature point of face, and fixed number of iteration gives the result of facial feature points tracking.

2.3 Classification

In classification, formulate the support vector machine (SVMs) with facial animation parameters (FAPs) of extracted feature points. Support vector machines (SVMs) [15, 16] are linear separating a maximum margin of hyperplane in a higher dimensionality space. Let $g_j = \{(\vec{x}_i, \vec{y}_i)\}; i = 1...k; \vec{x} \in \Re^n; y_i \in \{-1, +1\}$ is the training dataset of facial extraction of feature vectors displacement. Then maximum margin of separating hyperplane of linear data of the form is Eq. (4).

$$\begin{aligned} \vec{w}^T \cdot \vec{x} + b \geq +1 \quad \text{for } (y_i = +1) \\ \vec{w}^T \cdot \vec{x} + b \leq -1 \quad \text{for } (y_i = -1) \end{aligned} \tag{4}$$

$\vec{w}^T$ is weight vectors, where normal to the separating hyperplane and $\vec{w}^T$ is a bias. A decision function of separating hyperplane is as follows in Eq. (5).

$$f(\vec{x}) = \vec{w}^T \cdot \vec{x} + b \tag{5}$$

Subject to constraint inequalities is Eq. (6) the separating linear optimal hyperplane in form out Eq. (7) :

$$y_i\left(\vec{w}^T \cdot \vec{x}_i + b\right) - 1 \geq 0 \quad i = 1, \dots N \tag{6}$$

$$\vec{w} = \sum_{i=1} \alpha_i \cdot \tilde{S}_i \tag{7}$$

The two class of linear SVMs of decision surface is as follows in Eq. (8):

$$f(x) = \sigma\left(\sum_{i=1} \alpha_i \, \Phi(\tilde{S}_i) \cdot \Phi(x)\right) \quad \text{or} \quad y = \vec{w} \cdot x + b \tag{8}$$

From Eq. (8) gives the discriminating hyperplane of separating cluster in decision surface. For nonlinear case of SVMs, the training data are changed into linear separable data by using kernel function (polynomial, rbf), normalization and transformation of Φ mapping function [15, 16]. From Eq. (8), decision surface is classify the detecting happiness are seen detailed in Sect. 3.

3 Experimental Results and Discussion

3.1 Feature Vectors Displacement

The information of face detection, tracking and extraction are carried out for emotion in real-time human face using geometric deformable model (CLM) [14].

The extracted information of happiness is in frame-by-frame facial features movement to form the facial feature vectors displacement. The geometric information of feature vectors displacement is one node displacement $d_{i,j}$ defined as the consecutive frame-by-frame difference between the grid node displacements of first to ith node coordinates. The feature vectors displacement is in Eq. (9):

$$d_{i,j} = \begin{bmatrix} \Delta x_{i,j} \\ \Delta y_{i,j} \end{bmatrix} = \begin{pmatrix} a_{11} - a_{12} & a_{13} - a_{14} & \cdots & a_{1,j+1} - a_{1,j+2} \\ a_{21} - a_{22} & a_{23} - a_{24} & \cdots & a_{2,j+1} - a_{2,j+2} \\ \vdots & \ddots & & \vdots \\ a_{i,j} - a_{i,j+1} & \cdots & & a_{n,m+1} - a_{n,m+2} \end{pmatrix} \quad (9)$$

$i = 1, \ldots F, j = 1, \ldots N$, where $\Delta x_{i,j}$, $\Delta y_{i,j}$ are x-axis, y-axis coordinates of grid node displacement of the ith node in jth frame image, respectively. F is the number of grid node ($F = 66$ nodes of CLM), and N is the number of the extracted facial images from the facial image sequence.

$$g_j = \begin{bmatrix} d_{1,j} \, d_{2,j} \ldots d_{E,j} \end{bmatrix}^T \quad j = 1, \ldots N \quad (10)$$

From Eq. (10), for every sequence of the happy face in dataset, an extracted feature vectors grid deformation vector g_j is created to form the displacements of the every geometric grid node $d_{i,j}$. In happy face, major muscle variation is happening in mouth region (Groups 8 and 2 of FAPs). From the extracted features from CLM, feature vectors displacement is computed. The entire and minimal feature vectors displacement of happy in CLM is shown in Fig. 2a, b; the blue color indicates as happy. The happy variations are more in outer lip and corner lip region with along x-axis direction defined from the FAPs [12].

In this system, the entire feature vectors displacement has high data computation and less accuracy of variation in happy. In order to achieve less data computation and high accuracy, minimal feature displacement is used and desired result is obtained. In Fig. 2a, the entire feature vectors displacement has feature variation in Group 8 (outer mouth lip region) and Group 2 (corner lip region) from the FAPs description. In our proposed, the minimal feature vectors displacements have the feature variation only in Group 2 (corner lip region) as shown in Fig. 2b. In this system, the geometric deformable grid node (CLM) has $L = 66 * 2 = 132$ dimensions. In the feature vectors displacement of image sequence, where computed the $d_{i,j}$ displacements of CLM grid node in order to form in start at neutral face to expressed face (i.e. Initial frame to peak response of frame) and the expressed face to neutral state. The CLM feature vectors displacement g_j is employing for the classification of happy face using two classes of SVMs in our proposed system. In our proposed system, the detecting happiness of CLM is developed in C++ with open framework tool and SVMs which was implemented in Intel i5 processor. In training and testing processes, MMI facial expression standard database [19] and real-time emotions of video rate is 30 frames/s are respectively and only frontal face image sequence are captured are shown in Fig. 3.
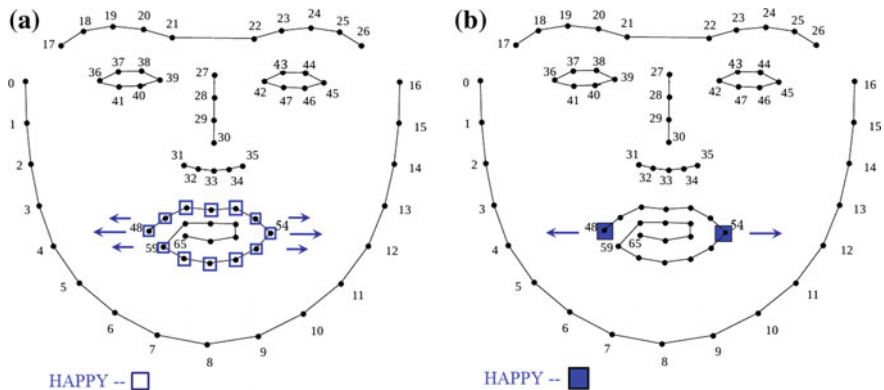
Fig. 2 CLM grid of entire and minimal feature vectors displacement of Happy

3.2 Training Process

In Happy, the major facial muscle movement in Group 8 and Group 2 of temporal segments in *x*-axis direction of the entire and minimal feature vectors displacement defined by FAPs [12]. From Fig. 4a, b are shown as expression value (i.e., offset-apex-onset region) of entire and minimal feature vectors displacements are respectively. In Happy, the major facial movement is horizontally expanded of both feature vectors. In that, the entire feature has taken all feature point for classification of happy. But it attained the high data computations with less accuracy. In order to achieve, the minimal feature vectors has only two feature points (49th and 55th of CLM grid node) for happy classification which attained the less data computations with high accuracy are shown in Fig. 4b. The reason for selecting minimal feature vectors, the two feature points have high variance compared to the outer lip mouth region (12 feature points) by FAPs.
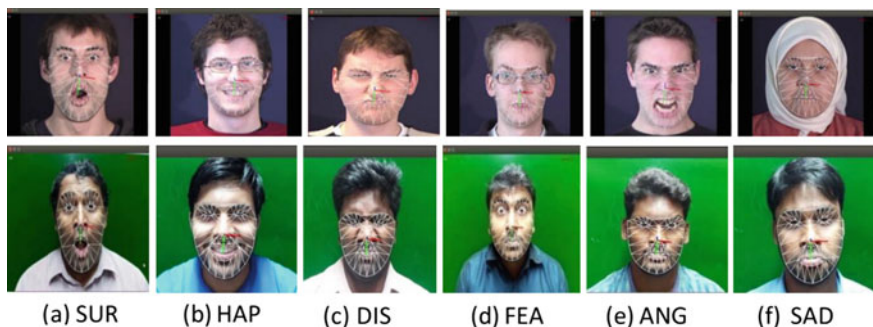
Fig. 3 Training and testing processes of MMI facial expression database (first row) and real-time (second row) facial expression datasets are respectively. **a** Surprise (SUR), **b** Happy (HAP), **c** Disgust (DIS), **d** Fear (FEA), **e** Anger (ANG), and **f** Sad (SAD).

In training process of happy classification, the entire and minimal feature vectors displacement of classification is shown in Fig. 4c, d. In that, trained 10 different subjects of happy (+ve class) and surprise (−ve class) were taken as bilinear SVMs are shown in Fig. 4c, d. In Fig. 4c, the entire feature vectors displacement of happy classification has attained the nonlinear data classification. In order to achieve linear classification of happy, applied the kernel function (polynomial, rbf), normalization and transformation of mapping function. In Fig. 4d, the minimal feature vectors displacement has conquered the linear separable datasets and also achieved less data computation with high accuracy.

3.3 Testing Process

In the testing process, the real-time facial data comprising of all basic six emotions were taken from 10 different subjects is shown in Fig. 3. Similarly, in the testing
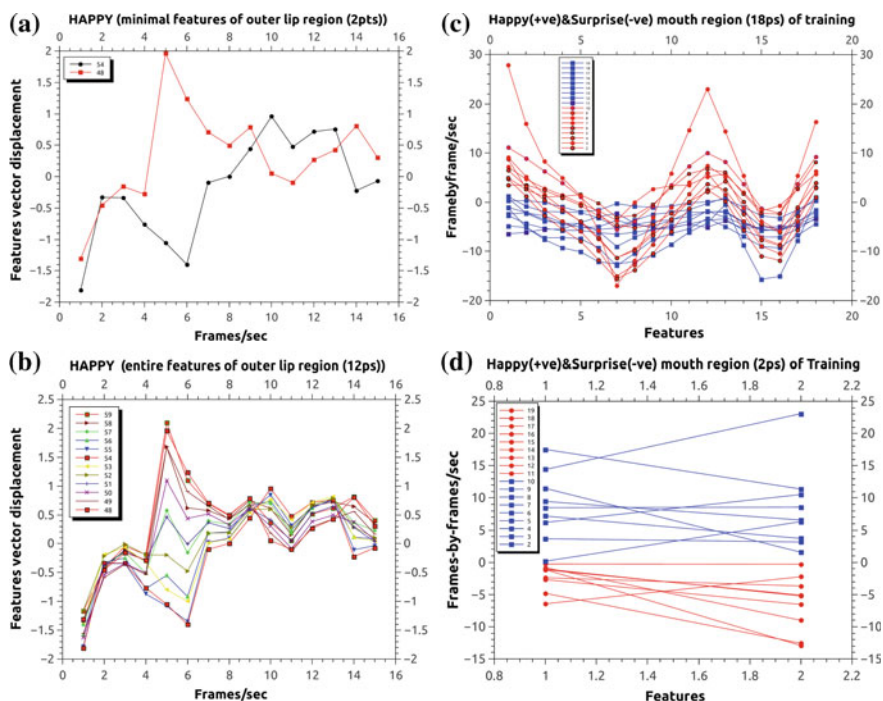
Fig. 4 **a** Entire feature vectors of Happy in outer lip corners (12 fps). **b** Minimal feature vectors of Happy in outer lip corner (48th and 54th fps). **c** Training process of happy (+ve) and surprise (−ve) of entire feature vectors of outer lip corners (12 fps) are in nonlinear case in bilinear SVMs. **d** Training process of happy (+ve) and surprise (−ve) of minimal feature vectors of outer lip corners (48th and 54th fps) are in linearly separable in bilinear SVMs

Table 1 Confusion matrix of Happy in bilinear SVMs classifier

EMO	HAP	SUR	SAD	FEA	ANG	DIS
HAP	10	0	0	0	0	0
SUR	0	10	0	0	0	0
SAD	0	0	10	0	0	0
FEA	1	0	0	9	0	0
ANG	2	0	0	0	8	0
DIS	2	0	0	0	0	8

process, where evaluated with the CLM face tracking and extracted features points to form the minimal features vectors displacement. The information of minimal feature vectors displacements was applied on the decision surface of trained model in the classification of happiness. The confusion matrix of Happy using bilinear SVMs is shown in Table 1. From the confusion matrix of happy, the overall accuracy is 91.66% achieved. The validation parameters are Precision is 3, Recall is 0.666, and *F*-measure values is 3 which is calculated from the confusion matrix of Happy.

4 Conclusion

In this paper, happiness is detected with minimal facial feature points using CLM and SVMs. In this system the minimal feature vectors are determined which contributes highly to detect happiness in human face. This leads to less computation and more accuracy. In this paper, the experiments are carried out with real time frontal facial expression and MMI Face expression database. Using minimal feature vector the accuracy of detecting happiness is 91.66% this work can be extends for the reminaing basic sets of emotion with multi-classification, different attributes (posed, spontaneous and wild), which helpful for developing HCI application.

References

1. Kollias S, Karpouzis K (2005) Multimodal emotion recognition and expressivity analysis. In: 2005 IEEE international conference on multimedia and expo. IEEE, pp 779–783
2. Ekman P, Sorenson ER, Friesen WV et al (1969) Pan-cultural elements in facial displays of emotion. Science 164(3875):86–88

3. Mase K (1991) Recognition of facial expression from optical flow. IEICE Trans Inf Syst 74(10): 3474–3483
4. Samal A, Iyengar PA (1992) Automatic recognition and analysis of human faces and facial expressions: a survey. Pattern Recogn 25(1):65–77
5. Bartlett MS et al (2003) Real time face detection and facial expression recognition: development and applications to human computer interaction. In: Conference on computer vision and pattern recognition workshop (CVPRW'03), vol 5. IEEE, pp 53–53
6. Lucey P et al (2010) The extended Cohn-Kanade dataset (CK+): a complete dataset for action unit and emotion-specified expression. In: 2010 IEEE computer society conference on computer vision and pattern recognition-workshops. IEEE, pp 94–101
7. Kotsia I, Pitas I (2007) Facial expression recognition in image sequences using geometric deformation features and support vector machines. IEEE Trans Image Process 16(1):172–187
8. Zhang Y et al (2008) Dynamic facial expression analysis and synthesis with mpeg-4 facial animation parameters. IEEE Trans Circuits Syst Video Technol 18(10):1383–1396
9. Pantic M, Patras I (2006) Dynamics of facial expression: recognition of facial actions and their temporal segments from face profile image sequences. IEEE Trans Syst Man Cybern Part B (Cybern) 36(2):433–449
10. Okada T, Takiguchi T, Ariki Y (2010) Video searching system based on human face identification and facial expression recognition using MSM and AAM. Far East J Electron Commun 4(1):41–48
11. Tian Y-I et al (2001) Recognizing action units for facial expression analysis. IEEE Trans Pattern Anal Mach Intell 23(2):97–115
12. Tekalp AM, Ostermann J (2000) Face and 2-D mesh animation in MPEG-4. Signal Process Image Commun 15(4):387–421
13. Salam H (2013) Multi-object modelling of the face. Ph.D. thesis, Supelec
14. Saragih JM et al (2011) Deformable model fitting by regularized landmark mean-shift. Int J Comput Vis 91(2):200–215
15. Ventura D (2009) SVM example. Lectures notes, Mar 2009
16. Vapnik VJ, Vapnik V (1998) Statistical learning theory, vol 1. Wiley, New York
17. Cristinacce D, Cootes TF (2006) Feature detection and tracking with constrained local models. In: BMVC, vol 1, p 3
18. Cheng Y (1995) Mean shift, mode seeking, and clustering. IEEE Trans Pattern Anal Mach Intell 17(8):790–799
19. Valstar M, Pantic M (2010) Induced disgust, happiness and surprise: an addition to the MMI facial expression database. In Proceedings of the 3rd international workshop on EMOTION (satellite of LREC): Corpora for research on emotion and affect, p 65

Analysis of Myocardial Ischemia from Cardiac Magnetic Resonance Images Using Adaptive Fuzzy-Based Multiphase Level Set

M. Muthulakshmi and G. Kavitha

Abstract In this research work, cardiac magnetic resonance (CMR) images are analyzed to study the pathophysiology of myocardial ischemia (MI). It is a cardiac disorder that causes irreversible damage to heart muscles. The images considered for this study are obtained from medical image computing and computer-assisted intervention (MICCAI) database. Adaptive fuzzy-based multiphase level set method is utilized to extract endocardium and epicardium of left ventricle from short-axis view of CMR images. The segmentation results are validated with similarity measures such as Dice coefficient and Jaccard index. Further, five indices are derived from the segmentation results. The obtained results provide average Dice coefficient for endocardium and epicardium as 0.867 and 0.918, respectively. The mean Jaccard index for epicardium and endocardium is 0.855 and 0.766, respectively. It is observed that the proposed method segments the left ventricle more precisely from CMR images. The ischemic subjects show a reduced mean ejection fraction (32.52) compared to the normal subjects (59.04). The average stroke volume is found to be 70.16 and 64.05 ml for healthy subjects and ischemic subjects, respectively. Reduction in stroke volume and ejection fraction for ischemic subjects indicates lower quantity of blood drained by heart. It is also observed that there is an increase in myocardial mass for ischemic subjects (182.11 g) compared to healthy subjects (127.47 g). The thickened heart muscle contributes to the increased myocardial mass in abnormal subjects. Further, ischemic subjects show an increase in endocardium volume at end-diastolic and end-systolic phase when compared to normal subjects. Thus, the clinical indices evaluated from adaptive fuzzy-based multiphase level set method could differentiate the normal and ischemic subjects. Hence, this study can be a useful supplement in diagnosis of myocardial ischemic disorder.

M. Muthulakshmi (✉) · G. Kavitha
Department of Electronics Engineering, MIT Campus, Anna University, Chennai, India
e-mail: lakshmingm.2@gmail.com

G. Kavitha
e-mail: kavithag_mit@annauniv.edu

1 Introduction

Myocardial ischemia (MI) is an irreversible cardiovascular disorder. Cardiovascular disease (CVD) is the predominant cause of fatality globally. MI is characterized by weakened heart muscles [1]. The interruption of blood supply damages the heart muscles that inhibit its ability to pump blood. Eventually, this may be captured as abnormal heart rhythms, diastolic and systolic dysfunctions [2]. MI causes chest pain, discomfort in shoulder, arm, back, neck, and jaw. Mortality due to acute myocardial ischemia can be reduced by diagnosis and treatment at an earlier stage.

Various modalities used to diagnose CVD include echocardiography, magnetic resonance images (MRI), computed tomography (CT), single photon emission computed tomography (SPECT), positron-emitted tomography (PET) and integrated modalities. The effective noninvasive modality for CVD diagnosis is cardiac magnetic resonance (CMR) images [3]. CMR provides high soft-tissue contrast, multiplanar acquisition capability and lacks ionizing radiations. Left ventricle (LV) segmentation from CMR is essential for quantitative cardiac study. Segmentation of LV manually done by radiologists are complex, consumes more time, and prone to human errors [4]. The papillary muscles make automatic segmentation of LV difficult as their intensities are similar to myocardium. Intensity inhomogeneity and reduced contrast between other organs and myocardium pose additional challenges in segmentation. Clinical indices such as left ventricle volume, ejection fraction, and mass are evaluated with the outcomes obtained from segmentation of LV echocardiographic images [5]. These indices aid the diagnosis of myocardial ischemia, and they can be computed more precisely with the aid of efficient segmentation algorithm.

Previous works on left ventricle segmentation are based on local or global information [6], deformable models [7], atlas [8], and statistical models [9]. The local information-based methods better segregate region of interest based on intensity of pixels. However, they are less effective when tissues have overlapping intensities [10]. The region growing algorithms though work better for less gradient images; the drawback is that they leak into irrelevant adjacent regions. Atlas-based methods require prior information that depends on spatial probability pattern of different tissues. The training time of statistical models depends on the training population. Furthermore, model-based methods preserve anatomical spatial information. Past studies revealed that active contour models provide promising approach for left ventricle segmentation [11]. Here, a contour deforms its shape in accordance with internal and external forces. LV segmentation of CMR images is carried out with active contour model coupled with nonlinear shape priors [12]. Li et al. introduced multiphase level set method to segment X-ray, CT and MR images with intensity inhomogeneity [13]. Recently, two-step DRLSE is applied for LV

and RV segmentation using CMR images [14]. In detection of cardiac ischemia, unsupervised support vector machine along with dictionary learning is carried out on CMR images dependent on blood oxygen level [15].

The limitation with majority of the segmentation methods based on active contour is that their precision depends on the appropriate placement of initial contour which requires manual intervention. In order to overcome this, Huang et al. initialized the contour for snake models utilizing fuzzy C-means clustering and graph-cut segmentation method [16]. Region-based level set method including fuzzy C-means clustering is applied to brain CT images for hemorrhage segmentation [17]. A fuzzy C-means clustering methodology that is adaptively regularized is implemented for brain tissue segmentation from MR brain images [18]. The initial contour obtained from adaptive fuzzy and the level set energy based on adaptive fuzzy membership function would provide more precise segmentation results.

In this work, a multiphase level set method based on adaptive fuzzy is employed for segmentation of endocardium and epicardium from CMR images. Fuzzy-based intensity descriptor is incorporated to define the energy of the multiphase level set function. The efficacy of the segmentation method is validated with similarity measures such as Jaccard index and Dice coefficient. From the segmented regions indices such as left ventricle end-diastole and end-systole volume, stroke volume, ejection fraction and myocardial mass are calculated. These indices could aid the diagnosis of cardiovascular disorders such as myocardial ischemia.

2 Material and Methods

2.1 Database

The short-axis cardiac magnetic resonance images used for the analysis are acquired from the medical image computing and computer-assisted intervention (MICCAI) left ventricle segmentation database [19]. The database contains cine-MR images of 45 patients from a range of pathology. The subjects are divided as normal, ischemic heart failure, non-ischemic heart failure and hypertrophy. Ground truths for evaluation purpose are provided by expert cardiologists. The description about age and gender of each subject is provided in the database.

2.2 Adaptive Fuzzy-Based Multiphase Level Set

Adaptive fuzzy-based multiphase level set (AFMLS) method is applied for segmentation of epicardium and endocardium of LV simultaneously. In multiphase level set method, k-level set contours $\Phi_1, \Phi_2, \ldots, \Phi_k$ are used and their membership

function is defined by $M_i(\Phi_1(y),\dots, \Phi_k(y))$ [13]. The energy of an AFMLS function [13, 17] is given by

$$\varepsilon(\Phi, c, b) = \int \sum_{i=1}^{N} e_i(x) M_i(\Phi(x)) dx. \tag{1}$$

where e_i is the energy-based intensity descriptor, the k-level set functions $\Phi_k(x)$ is defined by adaptive fuzzy membership function output u_{ij}, cluster center [18], and N is the number of segmented regions.

$$u_{ij} = \frac{\left(\left(1 - K(x_i, v_j)\right) + \varphi_i\left(1 - K(\bar{x}_i, v_j)\right)\right)^{-1/(m-1)}}{\sum_{k=1}^{c}\left(\left(1 - K(x_i, v_k)\right) + \varphi_i\left(1 - K(\bar{x}_i, v_k)\right)\right)^{-1/(m-1)}} \tag{2}$$

where φ is the adaptive regularization parameter, number of clusters denoted by c, K represents Gaussian radial basis kernel function, and m indicates the weighting exponent indicating the degree of fuzziness.

$$e_i = |I - bc_i|^2. \tag{3}$$

where $i = 1$ to N, original image is given by I, b represents bias field, and c denotes the cluster center. In this work, $N = 3$ is considered.

2.3 Similarity Measures

Segmentation outcomes are quantitatively evaluated using Dice coefficient and Jaccard index [10]. The similarity between the ground truth and computed segmentation results is evaluated by Dice coefficient and Jaccard index. The similarity measure has values in the range of 0–1. Higher value indicates better segmentation results. A_s is the segmented region using AFMLS method, and A_m is the ground truth.

3 Results and Discussion

The short-axis view CMR sequence of frames used in this work includes 9 normal and 12 ischemic subjects. Adaptive fuzzy-based multiphase level set (AFMLS) algorithm is applied for segmentation of epicardium and endocardium of left ventricle from CMR images. In this method, the value for level set parameters σ, timestep, μ, and υ are chosen as 7, 0.1, 1, and $0.01 * A^2$ where $A = 255$.

Figure 1a–h illustrates the endocardial and epicardial contours of left ventricle (LV) from end-diastole (ED) to end-systole (ES) phase for a normal subject.
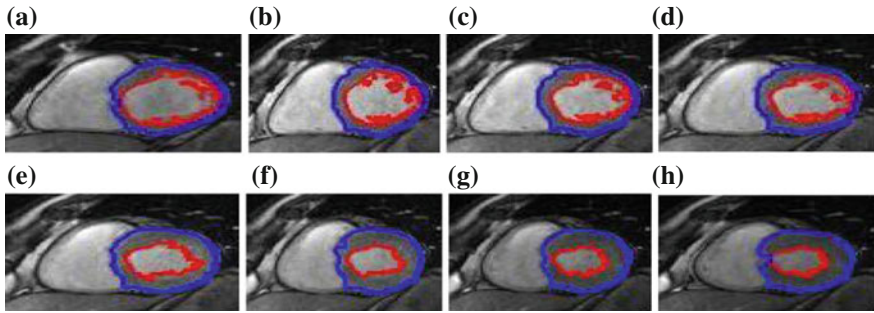
Fig. 1 AFMLS segmentation of left ventricle from ED phase to ES phase for normal subject. **a** ED image. **b**–**g** Progress from ED phase to ES phase. **h** ES image

Figure 1a corresponds to ED slice, and Fig. 1h corresponds to ES slice. The sequence of frames from ED to ES phase is shown in Fig. 1b–g. There is reduction in LV dimensions from ED phase to ES phase as the ventricle contracts. It is evident that the proposed AFMLS method could capture the variations in epicardial and endocardial geometry of LV from ED to ES phase.

The LV segmentation output at ED and ES phase using AFMLS method and ground truth for both normal and ischemic subjects is demonstrated in Figs. 2 and 3, respectively. Figure 2a–c shows the segmented endocardium during ED, epicardium during ED, and endocardium during ES for a healthy subject. The corresponding ground truth images for healthy subject are shown in Fig. 2d–f. The extracted endocardium at ED, epicardium at ED, and endocardium at ES for a ischemic subject are illustrated in Fig. 3a–c, respectively. Further, Fig. 3d–f illustrates the ground truth images for the same. Hence, it is evident that the proposed AFMLS algorithm is able to segment the endocardial and epicardial boundaries in both ischemic and normal subjects.

Fig. 2 a Segmented endocardium in ED phase. **b** Segmented epicardium in ED phase. **c** Segmented endocardium in ES phase. **d** Ground truth for endocardium in ED phase. **e** Ground truth for epicardium in ED phase. **f** Ground truth for endocardium in ES phase in normal subjects
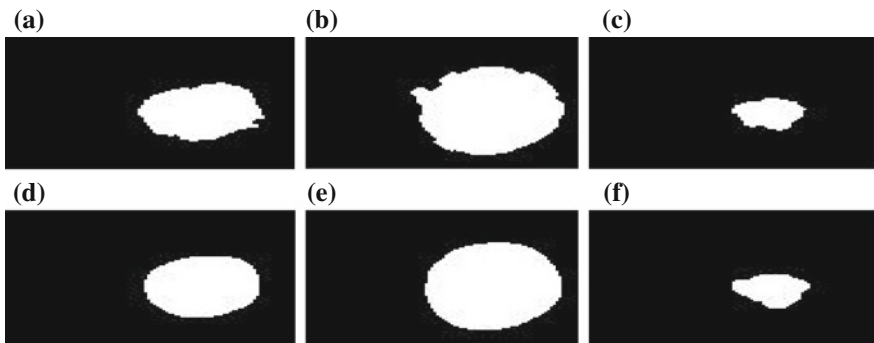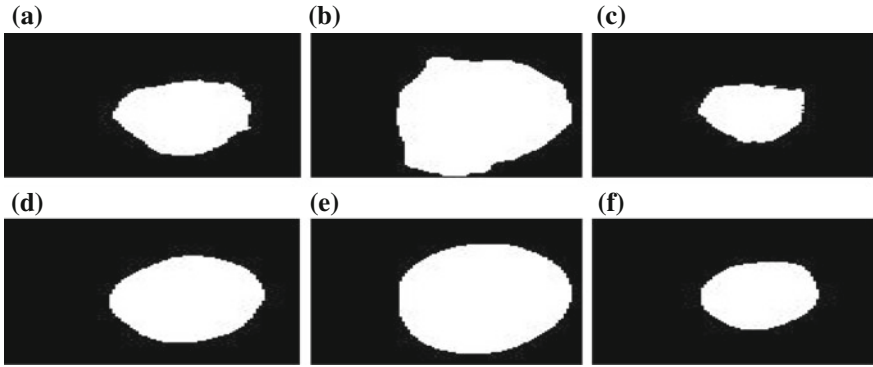
Fig. 3 a Segmented endocardium in ED phase. **b** Segmented epicardium in ED phase.
c Segmented endocardium in ES phase. **d** Ground truth for endocardium in ED phase. **e** Ground
truth for epicardium in ED phase. **f** Ground truth for endocardium in ES phase in ischemic subjects

The AFMLS algorithm is validated with the help of Dice coefficient and Jaccard index. The Dice metric calculates the overlapped area between the automatic segmentation result and the ground truth. The Dice coefficient obtained for different normal and ischemic subjects is shown in Fig. 4. The Dice coefficient for endocardium and epicardium segmentation of normal subjects is illustrated in Fig. 4a, b, respectively. Further, Fig. 4c, d shows the Dice coefficient for endocardium and epicardium segmentation of ischemic subjects. The mean Dice coefficient is obtained as 0.866 and 0.918 for endocardium and epicardium segmentation, respectively.

Figure 5 depicts the Jaccard index obtained for different normal and ischemic subjects. Figure 5a, b shows the Jaccard index for endocardium and epicardium segmentation of normal subjects, respectively. Further, the Jaccard index for endocardium and epicardium segmentation of ischemic subjects is illustrated in Fig. 5c, d, respectively. The average Jaccard index is 0.766 and 0.855 for endocardium and epicardium segmentation, respectively. It is observed from the similarity measures that the proposed AFMLS algorithm is able to segment the LV better from both normal and ischemic CMR images. Though the segmentation validation indices are high for both normal and ischemic subjects, the Dice coefficient and Jaccard index are relatively low for endocardium segmentation in ischemic subjects. This could be due to ill-defined edges in abnormal cardiac MR images. Fuzzy better clusters the regions when the edges are well defined.

The indices such as myocardial mass, ejection fraction, end-systole volume, end-diastole volume and stroke volume for normal and ischemic subjects are calculated for the segmented left ventricle [10]. Figure 6 shows end-diastole volume (EDV) for LV of normal and ischemic subjects, where the ventricle dilates. It is observed that there is an increase in the end-diastole volume for ischemic subjects compared to the normal subjects. This indicates an increase in quantity of blood intake by the heart. Figure 7 illustrates the end-systole volume (ESV) for LV of
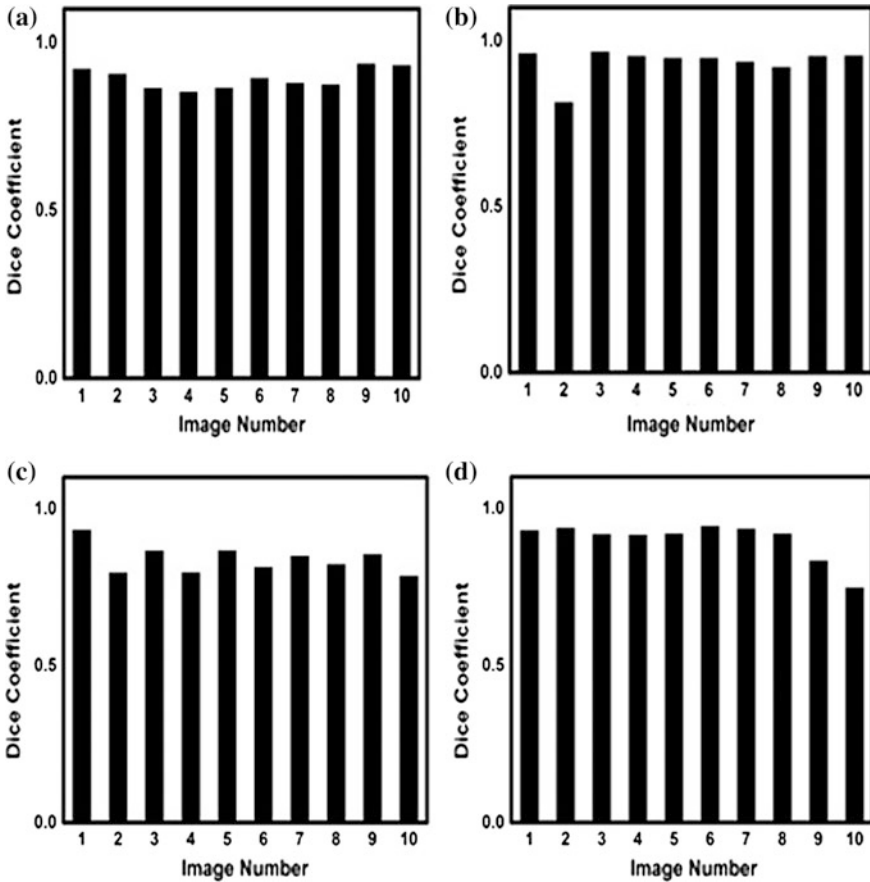
Fig. 4 Dice coefficient for **a** endocardium and **b** epicardium segmentation of normal subjects; **c** endocardium and **d** epicardium segmentation of ischemic subjects

normal and ischemic subjects, where the ventricle contracts. It is observed that the ESV shows a high range (90–180 ml) in ischemic subjects compared to normal subjects (40–80 ml). This analysis shows that the LV contraction is less in ischemic subjects and it is an indicator of systolic heart failure. In Fig. 8, the stroke volume (SV) for normal and ischemic subjects is shown. It is studied that the stroke volume reduces for ischemic subjects compared to normal subjects and it is more distributed in nature. The stroke volume is the difference in the EDV and ESV, which is an indicator of amount of blood drained by LV. Reduced SV indicates reduction in blood drained by the heart compared to normal subjects. It is associated with thickened myocardium and LV hypertrophy. Figure 9 shows the ejection fraction (EF) of left ventricle for normal and ischemic subjects. It is shown that the EF is low for ischemic subjects compared to normal subjects. The EF parameter well separates the ischemic and normal images. EF is the ratio of SV to EDV. Low EF